Two-Component Solution Processing of Oxide Semiconductors for Thin-Film Transistors via Self-Combustion Reaction

Young Hun Kang,‡ Sunho Jeong,‡ Jung Min Ko, Ji-Yoon Lee, Youngmin Choi, Changjin Lee,* and Song Yun Cho*

Additional Figures

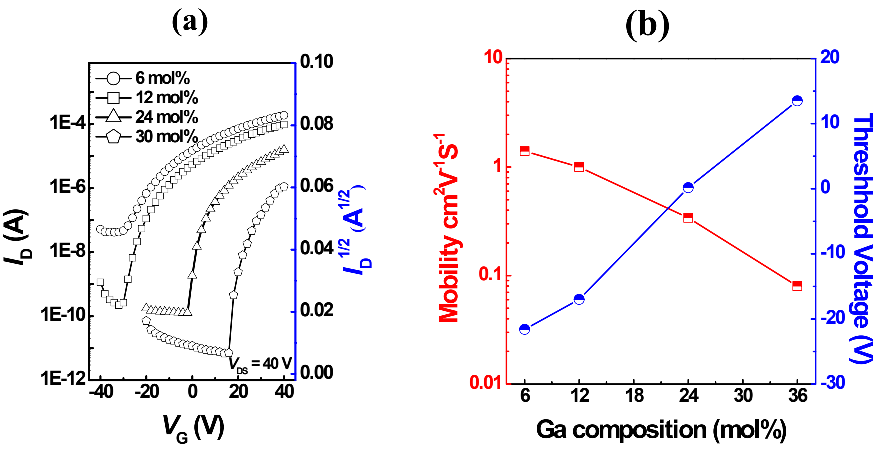

Fig. S1 (a) Transfer characteristics and (b) the variation of mobility and threshold voltage for fuel-free IGO TFTs depending on the chemical composition of In and Ga.

Table S1 The characteristics of IGO TFTs as a function of the composition of AcAc and NH_4OH

R value		Annealing temperature (^oC)	Average mobility ($cm^2 V^{-1} s^{-1}$)
Acetylacetone (R_1)	NH_4OH (R_2)		
1	1	250	0.20
		300	1.80
2	1	250	0.03
		300	0.96
1	2	250	0.21
		300	2.30
2	2	250	0.15
		300	3.55
3	2	250	0.04
		300	1.86
1	3	250	2.45
		300	12.50
2	3	250	0.23
		300	4.75
3	3	250	0.20
		300	Break down
1	4	250	1.10
		300	Break down
2	4	250	0.85
		300	Break down
3	4	250	0.70
		300	Break down

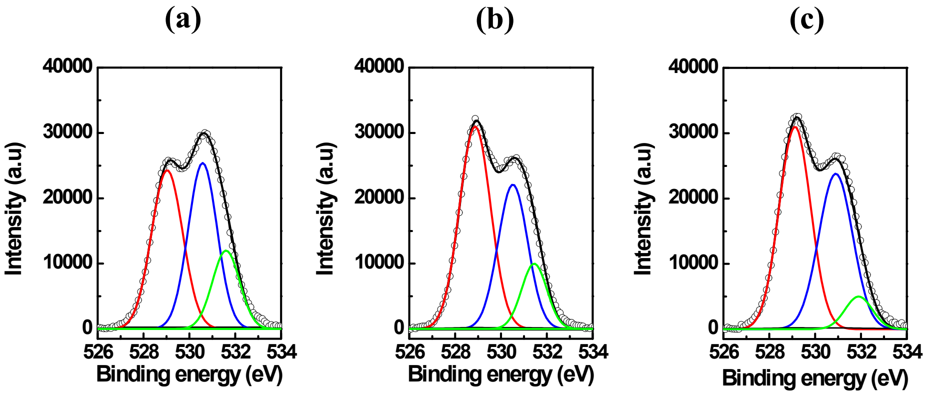

Fig. S2 XPS spectra of the $I_{NO}Z_{AC}O$ thin films at different annealing temperatures: (a) at 250 ^oC, (b) 300 ^oC, and (c) 350 ^oC.

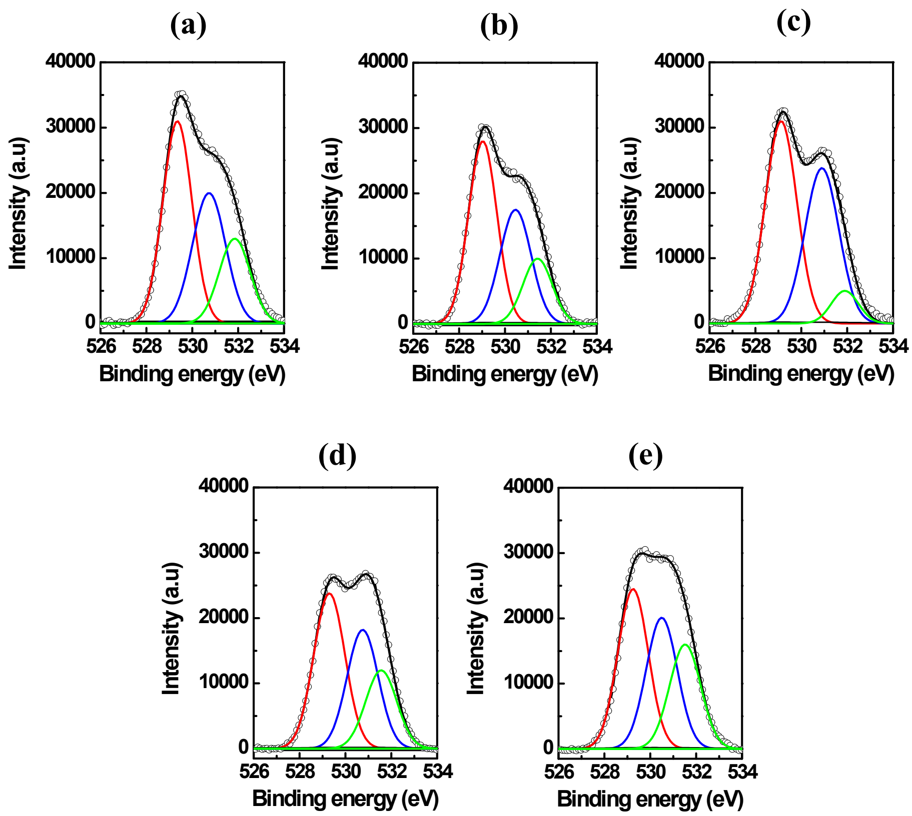

Fig. S3 XPS spectra of IZO thin films prepared from precursors with different composition ratios of In_{NO} to Zn_{AC}: (a) In_{NO}/Zn_{AC}=5/1, (b) In_{NO}/Zn_{AC}=4/2, (c) In_{NO}/Zn_{AC}=3/3, (d) In_{NO}/Zn_{AC}=2/4, and (e) In_{NO}/Zn_{AC}=1/5.

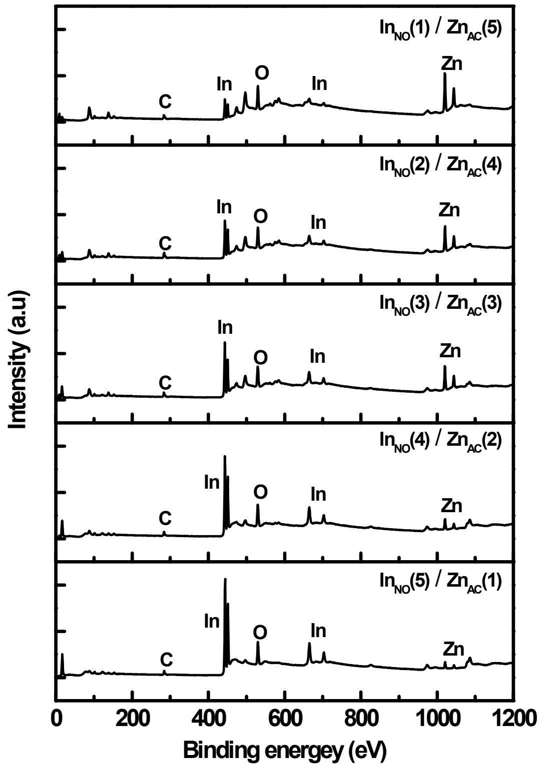

Fig. S4 XPS spectra of the $I_{NO}Z_{AC}O$ thin films from different composition ratios of In_{NO} to Zn_{AC} precursors.

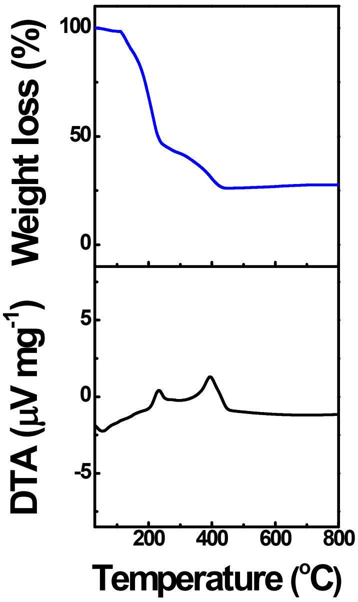

Fig. S5 Thermal behavior of the $I_{NO}Z_{AC}O$ precursor prepared from In_{NO}/Zn_{AC}=1/5.

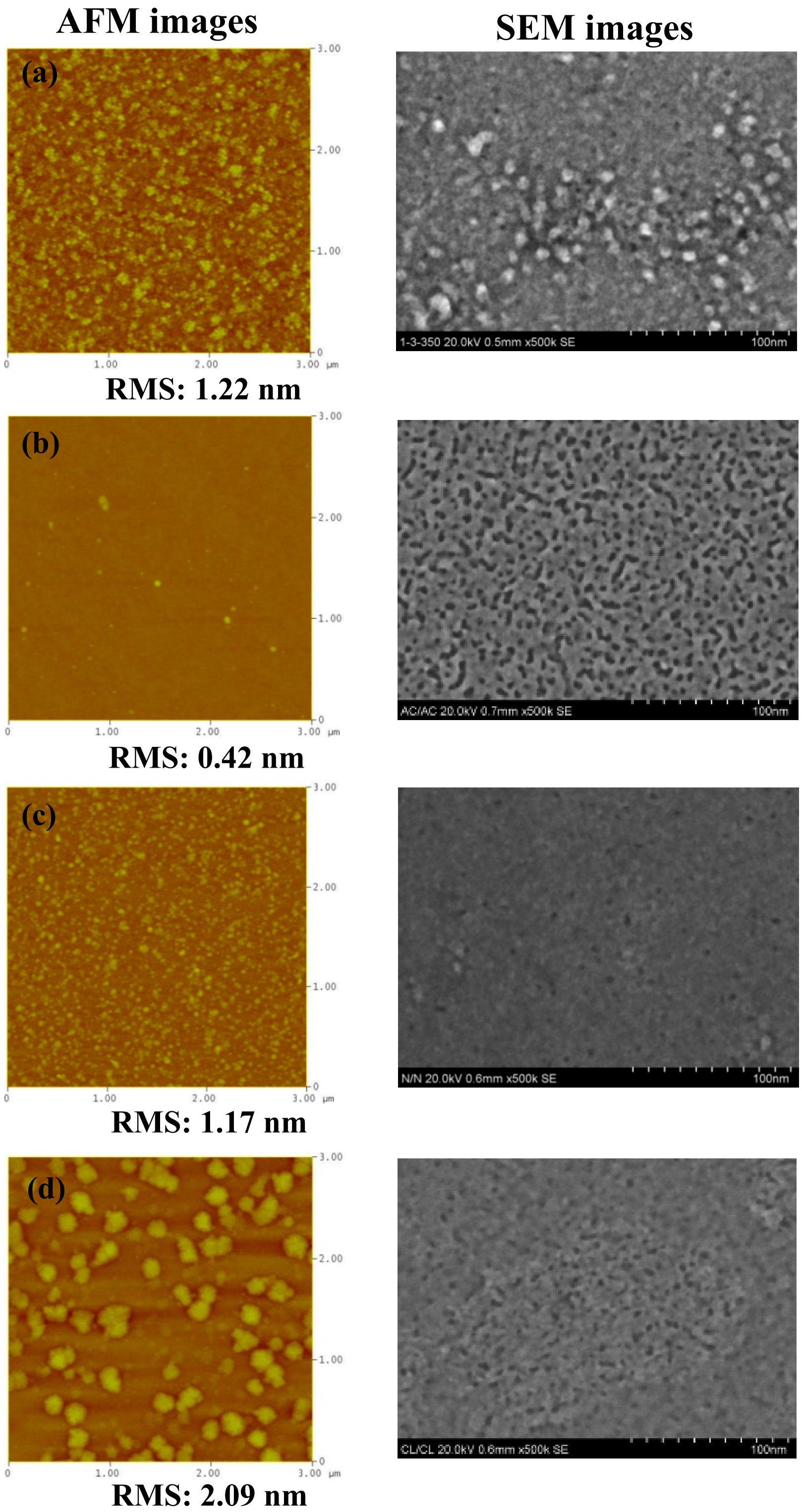

Fig. S6 AFM and SEM images showing the surface roughness of IZO thin films prepared from: (a) $I_{NO}Z_{AC}O$, (b) $I_{AC}Z_{AC}O$, (c) $I_{NO}Z_{NO}O$, and (d) $I_{Cl}Z_{Cl}O$ precursors.

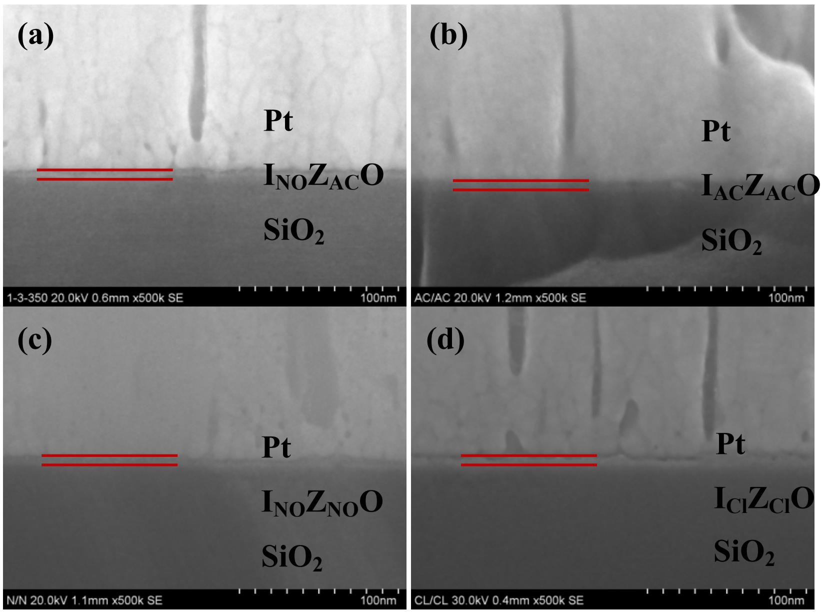

Fig. S7 Cross-sectional SEM images of the IZO thin films prepared from: (a) $I_{NO}Z_{AC}O$, (b) $I_{AC}Z_{AC}O$, (c) $I_{NO}Z_{NO}O$, and (d) $I_{Cl}Z_{Cl}O$ precursor.

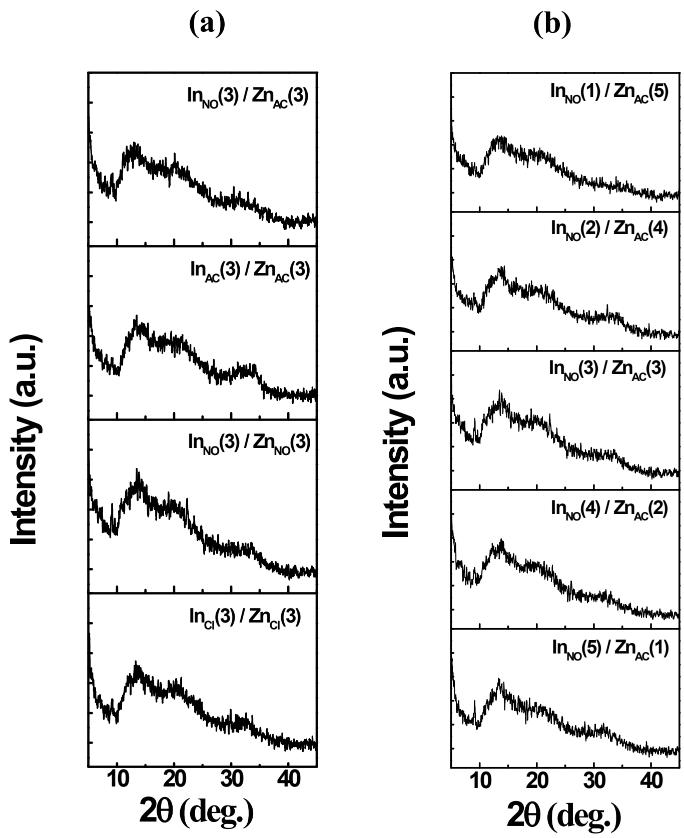

Fig. S8 XRD patterns of the IZO thin films according to the different (a) combinations and (b) compositions of In/Zn precursors.

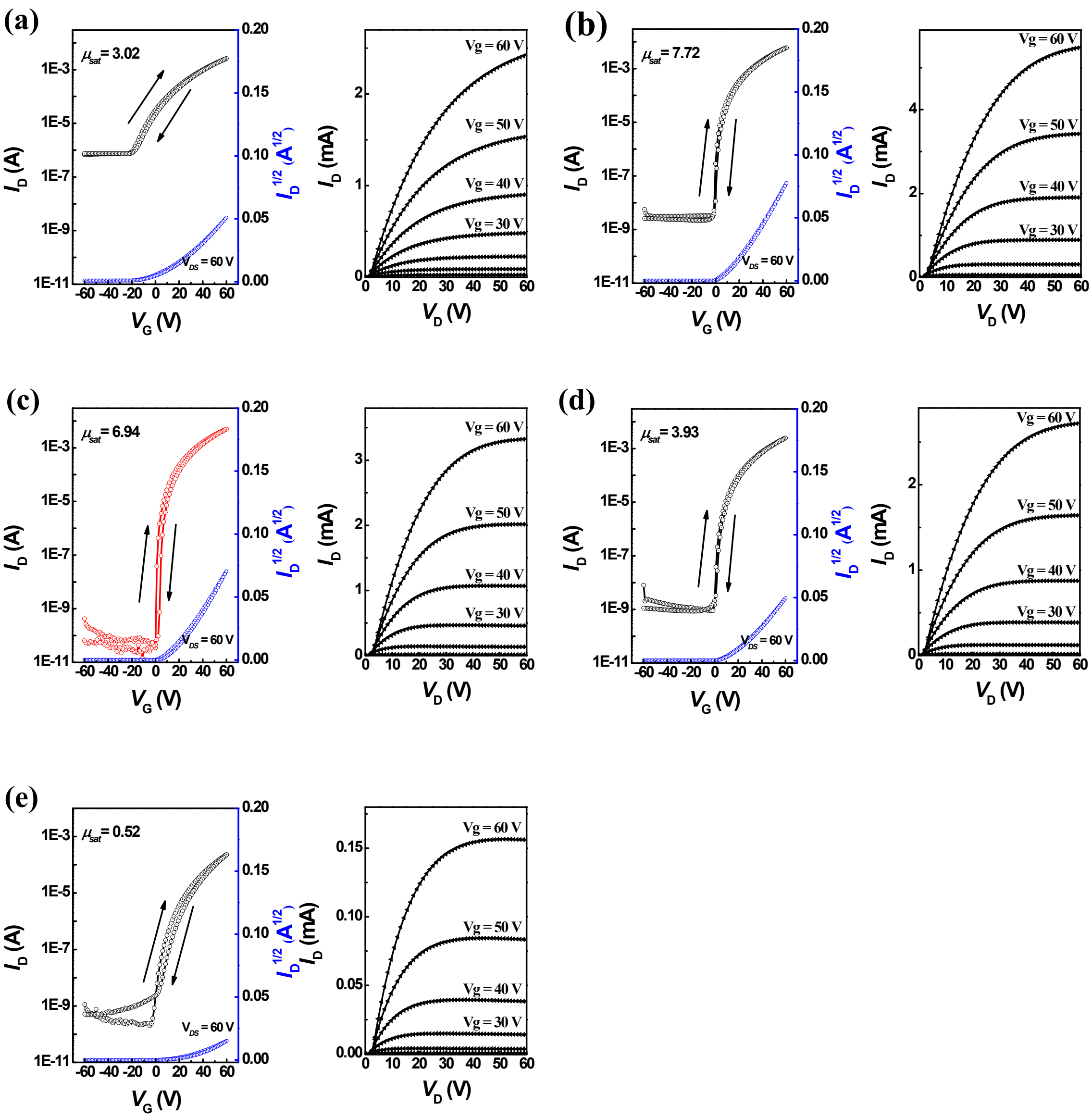

Fig. S9 The transfer and output characteristics of $I_{AC}Z_{NO}O$ TFTs fabricated from precursors with different composition ratios of In_{AC} to Zn_{NO}: (a) In_{AC}/Zn_{NO}=5/1, (b) In_{AC}/Zn_{NO} =4/2, (c) In_{AC}/Zn_{NO}=3/3, (d) In_{AC}/Zn_{NO}=2/4, and (e) In_{AC}/Zn_{NO}=1/5.

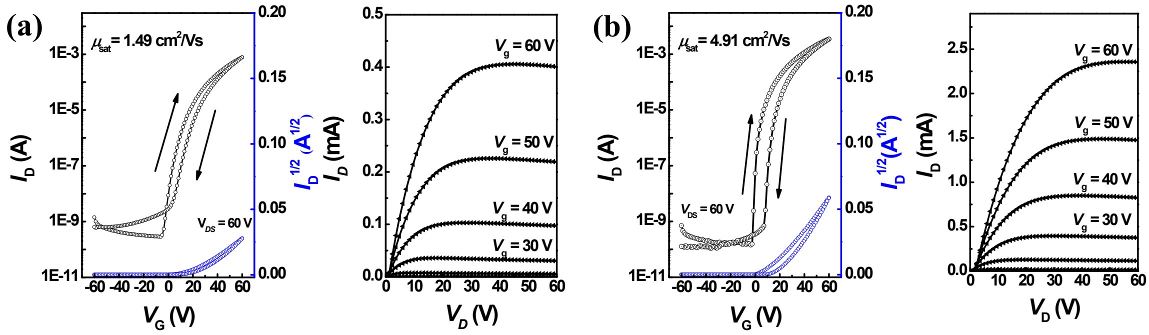

Fig. S10 The transfer and output characteristics of the $I_{NO}Z_{AC}$OTFTs at different annealing temperatures: (a) at 250 °C and (b) 300 °C.

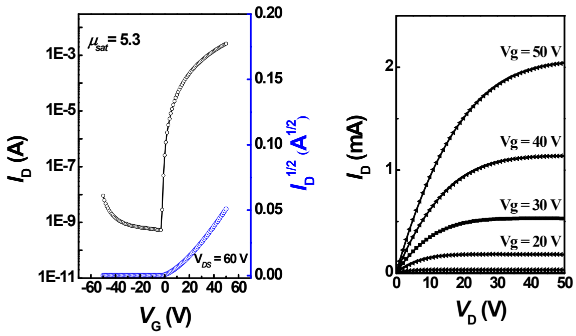

Fig. S11 The transfer and output characteristics of the inkjet-printed $I_{NO}Z_{AC}O$ TFT prepared with an identical composition ratio of In and Zn at annealing temperature of 350 °C.

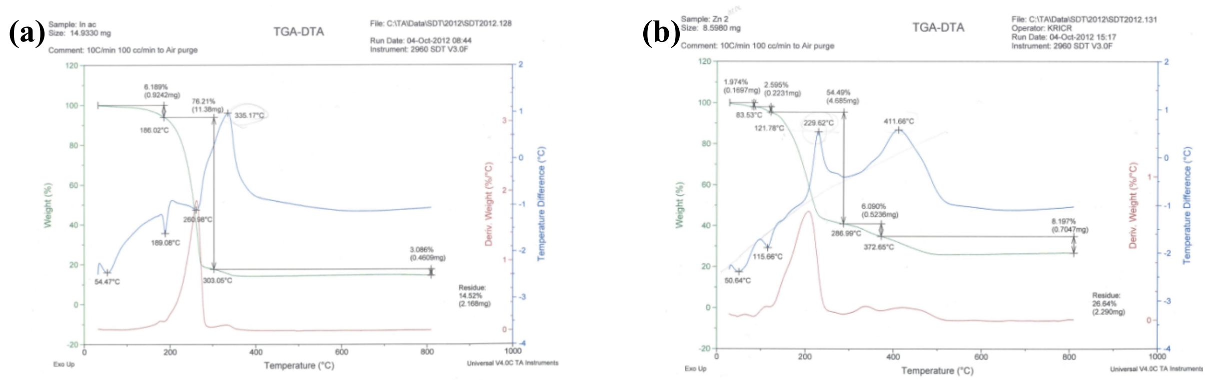

Fig. S12 Raw TGA and DTA thermogram of (a) In_{AC} and (b) Zn_{AC}.

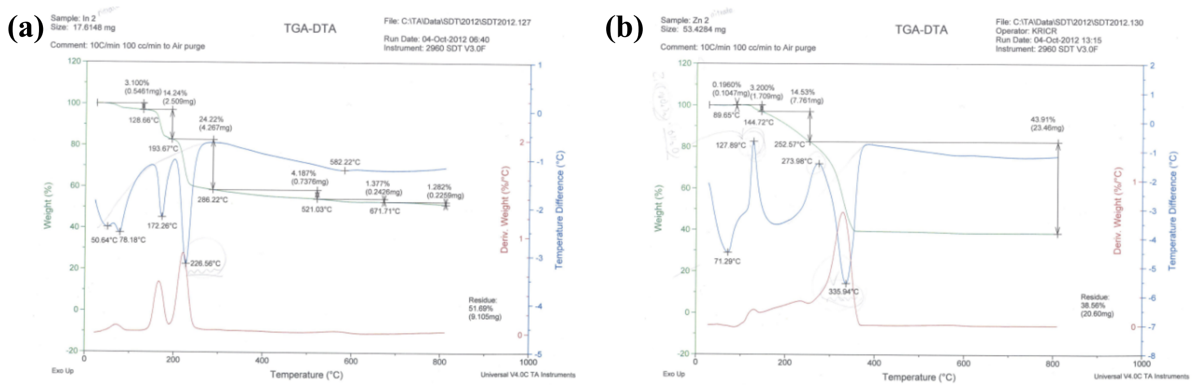

Fig. S13 Raw TGA and DTA thermograms of (a) In_{NO} and (b) Zn_{NO}.

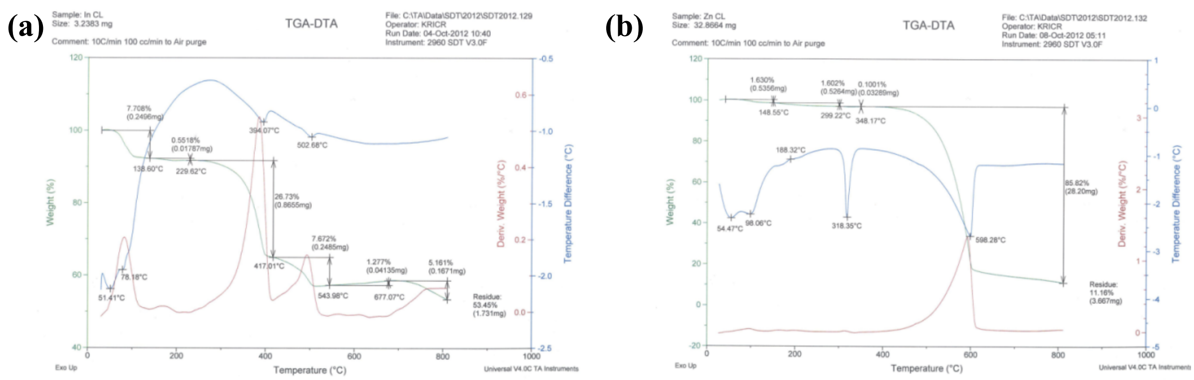

Fig. S14 Raw TGA and DTA thermograms of (a) In_{Cl} and (b) Zn_{Cl}.

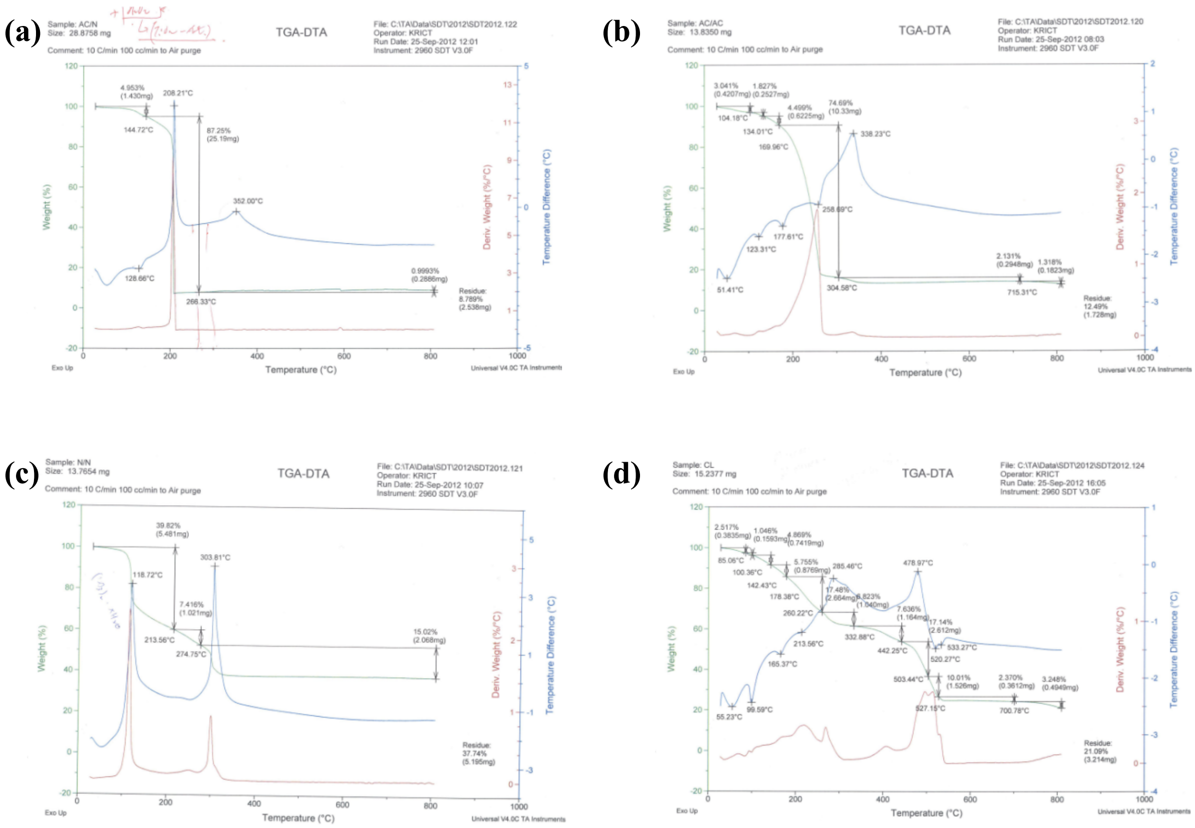

Fig. S15 Raw TGA and DTA thermograms of (a) $I_{NO}Z_{AC}O$, (b) $I_{AC}Z_{AC}O$, (c) $I_{NO}Z_{NO}O$ and (d) $I_{Cl}Z_{Cl}O$.